https://doi.org/10.5194/acp-2021-521
Preprint. Discussion started: 27 July 2021

Atmospheric Chemistry and Physics Discussions

Global maps of aerosol single scattering albedo using combined CERES-MODIS retrieval

Archana Devi[1], Sreedharan K Satheesh[1,2,3]

[1] Centre for Atmospheric and Oceanic Sciences, Indian Institute of Science, Bengaluru, India
[2] Divecha Centre for Climate Change, Indian Institute of Science, Bengaluru, India
[3] DST Centre of Excellence in Climate Change, Indian Institute of Science, Bengaluru, India

Correspondence to: Archana Devi (archana.shiva13@gmail.com)

Abstract. Single Scattering Albedo (SSA) is a leading contributor to the uncertainty in aerosol radiative impact assessments. Therefore accurate information on aerosol absorption is required on a global scale. In this study, we have applied a multi-satellite algorithm to retrieve SSA using the concept of 'critical optical depth.' Global maps of SSA were generated following this approach using spatially and temporally collocated data from Clouds and the Earth's Radiant Energy System (CERES) and Moderate Resolution Imaging Spectroradiometer (MODIS) sensors on board Terra and Aqua satellites. The method has been validated using the data from aircraft-based measurements of various field campaigns. The retrieval uncertainty is $\pm$0.03 and depends on both the surface albedo and aerosol absorption. Global mean SSA estimated over land and ocean is 0.93 and 0.97, respectively. Seasonal and spatial distribution of SSA over various regions are also presented. The global maps of SSA, thus derived with improved accuracy, provide important input to climate models for assessing the climatic impact of aerosols on regional and global scales.

1 Introduction

Atmospheric aerosols play a significant role in the Earth's radiation budget (IPCC, 2013). The climatic impact of aerosols depends on their absorption and scattering properties, quantified by Single Scattering Albedo (SSA). Even a slight reduction in SSA can change the aerosol radiative forcing from cooling to warming, depending on the underlying surface albedo (Kaufman et al., 2001; Chand et al., 2009). However, the lack of an accurate global aerosol absorption database has led to SSA being the largest contributor to the total uncertainty in aerosol radiative impact assessment (IPCC, 2013).

The high spatio-temporal variability in aerosol properties entails the need for observations on a global scale (Dubovik et al., 2002; Levy et al., 2007; Remer et al., 2008; Hammer et al., 2018). Satellite data, despite its

https://doi.org/10.5194/acp-2021-521
Preprint. Discussion started: 27 July 2021

Atmospheric Chemistry and Physics Discussions

inherent limitation associated with an inverse problem, can provide the global perspective required in analysing spatio-temporal aerosol characteristics (Torres et al., 2002; Lenoble et al., 2013). However, it is difficult to quantify the absorption over bright surfaces (Kaufman and Joseph, 1982; Ahn et al., 2014; Jethva et al., 2018). Hence, quantifying the aerosol absorption over land regions using satellite-based remote sensing remains a challenge even now (Torres et al., 2013; Jethva and Torres, 2019).

Various studies have ascertained the inadequacy of single-sensor data in the accurate retrieval of aerosol absorption (Kaufman et al., 2001; Zhu et al., 2011). Dawn of the A-Train satellite constellation (Anderson et al., 2005) with spatially and temporally near-collocated observations facilitates multi-satellite retrieval of aerosol absorption (Eswaran et al., 2019; Hsu et al., 2000; Hu et al., 2007, 2009; Jeong and Hsu, 2008; Narasimhan and Satheesh, 2013; Satheesh et al., 2009) However, all these multi-sensor retrievals are in the Ultra Violet (UV) wavelengths, and SSA is extrapolated to visible wavelengths using spectral dependence of assumed particle size distribution. Satheesh and Srinivasan (2005) defined the concept of "critical optical depth" (τ_c) and introduced a method to retrieve SSA in the visible region by combining ground-based and satellite measurements. The method was validated/demonstrated over many locations, including the desert location of Solar Village in Saudi Arabia, using Aerosol Robotic Network (AERONET) data.

In this paper, we have utilized the concept of τ_c and further extended the methodology to develop the combined CERES-MODIS retrieval algorithm to derive regional and global maps of aerosol absorption (550 nm) using multi-satellite data. The concept of τ_c, which forms the scientific basis for the development of this retrieval algorithm is illustrated in Section 2. The various steps involved in the retrieval algorithm are detailed in the Section 3, data and methodology. Section 4 presents the validation of SSA derived using this approach using aircraft measurements from various field campaigns. The global maps of SSA thus retrieved, its comparison with SSA from Ozone Monitoring Instrument (OMI), and the seasonal distribution of SSA over many regions are presented in Section 5. Summary and conclusions are provided in Section 6.

2 Critical optical depth

Let $\Delta\alpha$ be the difference between the top of the atmosphere (TOA) albedo and surface albedo. Then, for a particular location, with a given surface albedo, $\Delta\alpha$ variations are only due to changes in TOA albedo. The presence of absorbing aerosols over a bright surface decreases the TOA albedo. In contrast, scattering aerosols over a dark surface increase the TOA albedo. Thus, the increase (decrease) in aerosol loading due to scattering

https://doi.org/10.5194/acp-2021-521
Preprint. Discussion started: 27 July 2021

Atmospheric Chemistry and Physics
Discussions

(absorbing) type of aerosols leads to an increase (decrease) in Δα. The rate of change in Δα with aerosol loading is dependent on SSA.

Satheesh and Srinivasan (2005) utilized this concept to retrieve SSA in the case of absorbing aerosols over a bright surface. In a pristine atmosphere (Aerosol Optical Depth = 0) over a bright surface, the Δα is positive for solar zenith angle (SZA) = 0. Here, when absorbing aerosols become dominant, Δα decreases with an increase in aerosol optical depth (AOD) and eventually turns negative. The AOD at which Δα equals zero is defined as τ_c. For a given surface albedo, τ_c is the AOD at which the scattering and absorbing effects of the aerosol cancel each other. The rate of decrease in Δα with the increase in AOD is higher when SSA is high and consequently lowers the resulting values of τ_c. A radiative transfer (RT) model was then used to calculate the SSA that reproduces the same τ_c, given atmospheric conditions.

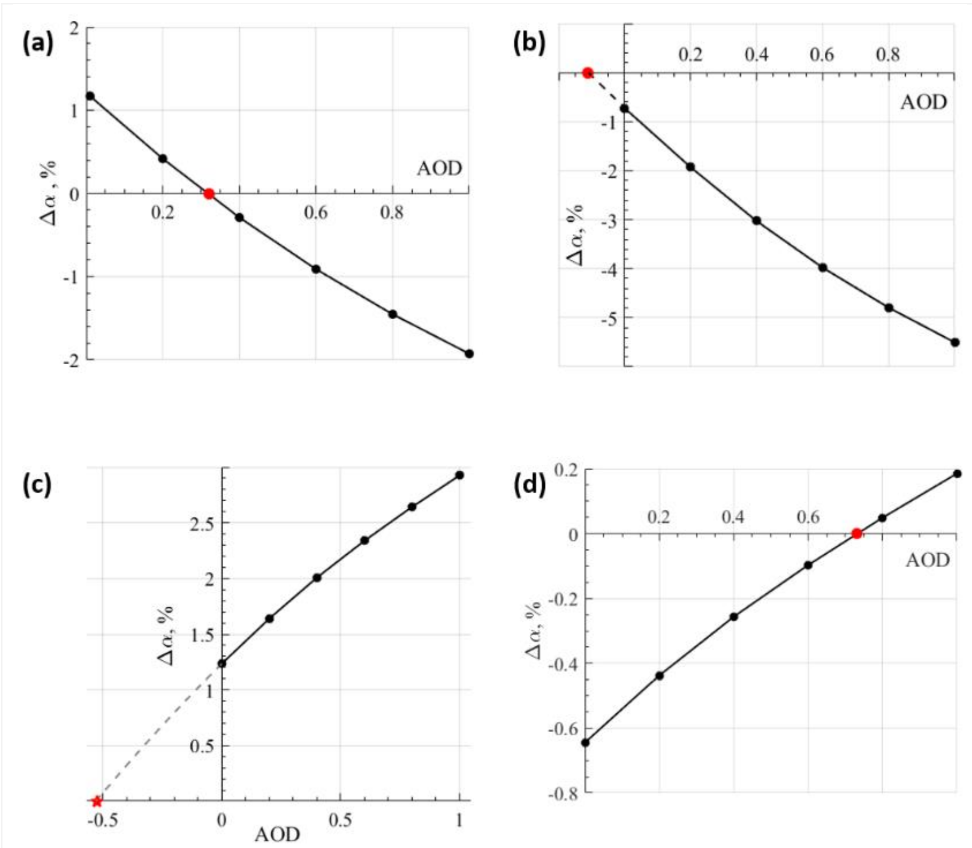

Figure 1. RT simulations (black dots) shows deriving τ_c (red dot) for different cases of aerosols and surfaces. For pristine conditions (AOD = 0), diurnally-averaged Δα is negative for bright surfaces and positive for dark surfaces.

https://doi.org/10.5194/acp-2021-521
Preprint. Discussion started: 27 July 2021

An increase in aerosol loading by absorbing (scattering) type of aerosol leads to decrease (increase) in TOA albedo. **(a)** Absorbing aerosols above a dark surface; **(b)** Absorbing aerosols above a bright surface; **(c)** Scattering aerosols above a dark surface; **(d)** Scattering aerosols above a bright surface.

In this paper, the concept of τ_c is extended to retrieve SSA for all scenarios of surfaces (dark and bright) and aerosols (absorbing and scattering). For AOD less than 1, $\Delta\alpha$ is almost linearly dependent on AOD. Then τ_c is mathematically the x-intercept when parameterizing the linear relationship.

Figure 1 shows the estimation of τ_c for four different scenarios. Details of these RT simulations are given in Section 3.2. Unlike Satheesh and Srinivasan (2005), where simulations were carried out for SZA = 0, here the $\Delta\alpha$ is diurnally averaged. Therefore, it is possible to have negative $\Delta\alpha$ for AOD = 0 over relatively bright surfaces. It is difficult to retrieve SSA where the slope of regression line is close to zero.

3 Data and methodology

The Combined CERES-MODIS retrieval algorithm consists mainly of two steps: (1) determining τ_c using MODIS and CERES data for a location, and (2) estimation of SSA that reproduces the same τ_c for the associated atmospheric conditions and surface albedo of that particular location. Figure 2 shows the flowchart illustrating the combined CERES-MODIS retrieval algorithm.

TOA and surface fluxes, used to determine $\Delta\alpha$, are obtained from CERES SYN1deg-day (Edition 4.1) (Wielicki et al., 1996; Rutan et al., 2015). To avoid angular dependence of fluxes, the diurnally averaged flux data product from CERES is used, which is available only at 1° resolution. Hence, other satellite data sets in this study are also used at the same spatial resolution. AOD and total columnar water vapor are obtained from the MODIS Daily Global Product (MxD08_D3 version 6.1). MODIS retrieves columnar AOD at 550 nm using two different types of algorithms – "Dark Target" (Levy et al., 2007, 2013) and "Deep Blue" (Hsu et al., 2004, 2006; Sayer et al., 2013). Dark target retrieves AOD over both land and ocean, whereas deep blue retrieves only over land. In this study, we have used a combined dark target and deep blue product.

https://doi.org/10.5194/acp-2021-521
Preprint. Discussion started: 27 July 2021

Atmospheric Chemistry and Physics Discussions

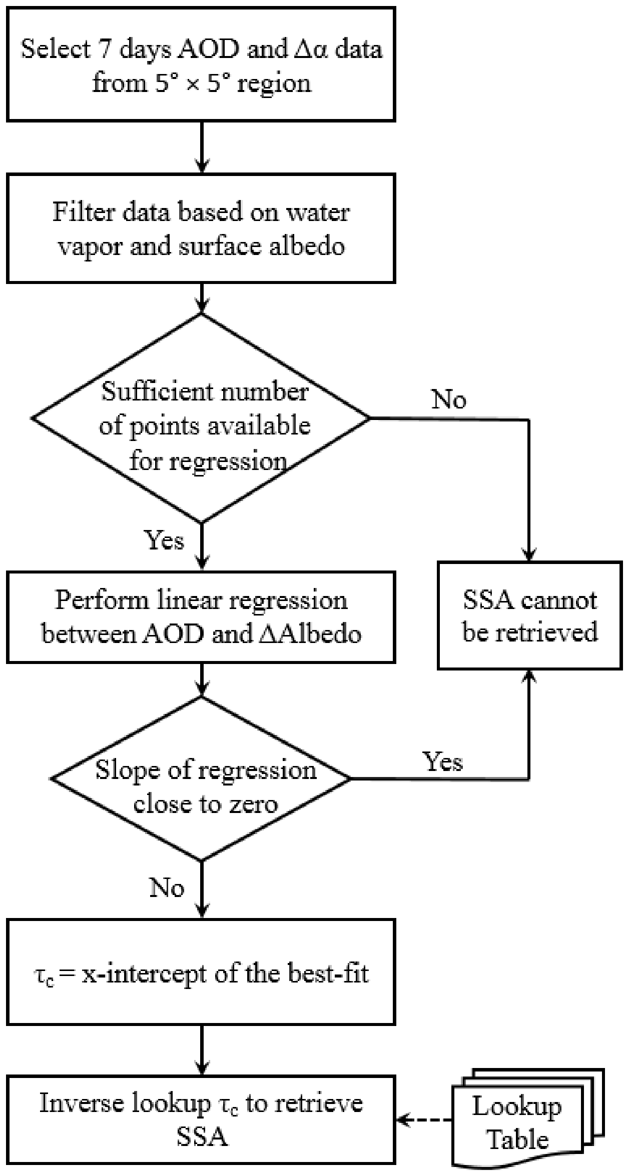

Figure 2. Flowchart depicting the steps involved in combined CERES-MODIS retrieval of SSA for a particular location.

3.1 Determining the critical optical depth

The first step for retrieval is to determine τ_c by linear regression analysis between $\Delta\alpha$ vs. AOD as shown in Fig. 3. The x-intercept of the resultant line of best fit (i.e., the AOD at which $\Delta\alpha = 0$) provides the value of τ_c. CERES

https://doi.org/10.5194/acp-2021-521
Preprint. Discussion started: 27 July 2021

and MODIS daily data are at 1° resolution, and SSA is retrieved for each 1° × 1° grid. In order to have adequate number of points for a meaningful regression analysis, it was required to use data over a larger interval (temporal and spatial) - whose extent is large enough to get a statistically significant fit but small enough to ensure insignificant variations in SSA. Thus, to determine τ_c for a given pixel, seven days of data from its surrounding 5° × 5° region has been considered. This data is further constrained based on surface albedo and water vapor. Only those pixels in this region having surface albedo within $\pm$ 0.025 and water vapor within $\pm$ 0.25 cm of the given pixel are considered for regression analysis. These constraints ensure that the τ_c determined from the best fit is dependent only on SSA and not affected by changes in surface albedo and water vapour. Figure 3a shows an example of regression with a positive correlation coefficient over the Arabian Sea. This can happen over regions of low surface albedo and the dominance of scattering aerosols. Figure 3b is an example of regression analysis with a negative correlation coefficient obtained over Sahara in the presence of dust aerosols.

The above procedure is repeated for all pixels, where data from the surrounding 5° × 5° region is used to determine τ_c for each pixel. For the regression analysis, points which are outside one standard deviation are considered as outliers. Line of best fits with a slope close to zero yields extreme τ_c values (very high positive/very low negative). In such cases, we did not attempt a retrieval. Only those τ_c values that are statistically significant at 95% confidence level are utilised further for the retrieval of SSA.

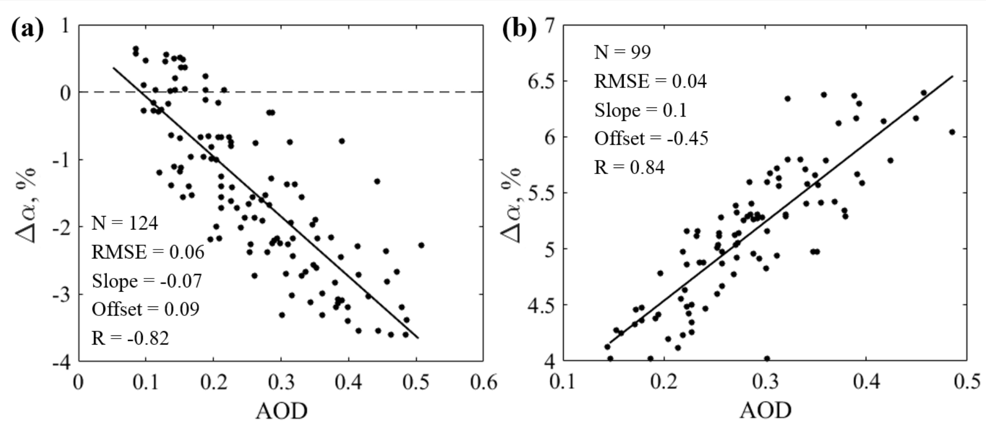

Figure 3. Sample scatterplots between MODIS AOD and CERES Δα. The solid lines represent the best-fits for **(a)** absorbing aerosols above the Sahara and **(b)** scattering aerosols above the Arabian Sea. τ_c (AOD at which Δα is zero) is the x-intercept of the best-fit line.

https://doi.org/10.5194/acp-2021-521
Preprint. Discussion started: 27 July 2021

The final product of this step is a 360 × 180 matrix that stores τ_c value corresponding to each 1° pixel. In these matrices, not all points would have a τ_c value owing to the insufficient number of points available for regression, either due to cloud-masking or large variations in surface albedo over the land. At least seven days of data is required to perform a statistically significant fit to compute τ_c and retrieve SSA The next step in the procedure is to estimate SSA from these τ_c values using an inverse lookup table (LUT) approach.

3.2 Retrieval of SSA

Since the objective of this study is to retrieve SSA globally, look-up-tables (LUTs) were developed to reduce the computation time and avoid repeated RT simulations. The aerosol models from OPAC (Optical Properties of Aerosols and Clouds), developed by Hess et al., (1998), are given as input to SBDART (Santa Barbara DISORT Atmospheric Radiative Transfer) model (Ricchiazzi et al., 1998) to simulate TOA fluxes.

The RT computations were carried out to obtain the diurnally averaged (SZA: 0° to 84°) TOA and surface fluxes using 16 radiation streams and spectrally integrated over the shortwave region (0.3 to 5 µm). For a particular case of surface albedo, water vapor, and SSA, AOD is varied from 0 to 1 in steps of 0.2 to generate its corresponding diurnally averaged $\Delta\alpha$. Then a linear fit is performed between AOD and simulated $\Delta\alpha$ to determine τ_c. A three-dimensional LUT that stores τ_c for different combinations of surface albedo, water vapor, and SSA have been developed. The LUT is indexed by 11 values of surface albedo (0 to 0.5, increments of 0.05), 17 values of water vapour (0 to 8 cm, increments of 0.5 cm) and 10 values of SSA (0.8, 0.83, 0.85, 0.87, 0.9, 0.92, 0.95, 0.97, 0.99, and 1). A total of 89760 RT simulations were performed in the present study.

The next step is to estimate SSA from τ_c using the LUT. For a given surface albedo and water vapor of that pixel, we find the SSA associated with its determined τ_c. An inverse lookup operation is performed on LUT by linear interpolation between the nearest two indices. SSA is estimated for each available τ_c values of a pixel and then averaged to compute the seasonal mean SSA.

4 Validation

For the validation of SSA values thus retrieved, we have used aircraft-based measurements of SSA from three campaigns: South West Asian Aerosol Monsoon Interactions (SWAAMI), Regional Aerosol Warming Experiment (RAWEX), and SWAAMI-RAWEX, to obtain column-integrated SSA. Available data points over

https://doi.org/10.5194/acp-2021-521
Preprint. Discussion started: 27 July 2021

Atmospheric Chemistry and Physics Discussions
Open Access
EGU

India and adjoining oceanic regions (Arabian Sea and Bay of Bengal) from these field campaigns were used to validate the retrieved SSA.

Babu et al. (2016), as part of RAWEX (Moorthy et al., 2016), derived SSA at 520 nm from aircraft measurements of scattering and absorption coefficients over the Indo-Gangetic Plain (IGP) and Central India during winter 2012 and spring/pre-monsoon 2013. Manoj et al. (2019) estimated vertical profiles of SSA during the SWAAMI campaign conducted during monsoon (June - July) 2016 over IGP, Arabian Sea, and Bay of Bengal. Vaishya et al. (2018) estimated vertical profiles of SSA (520 nm) using an instrumented aircraft, during SWAAMI-RAWEX campaign (June 2016).

Retrieved SSA, for the same period as the campaign, over a 2°×2° region around the campaign location was utilized for validation. Figure 4 shows the comparison of collocated aircraft measurements and CERES-MODIS retrieved SSA. The ideal 1:1 case (solid line), the absolute difference of 0.03 (dotted lines), and regression coefficients are also provided.

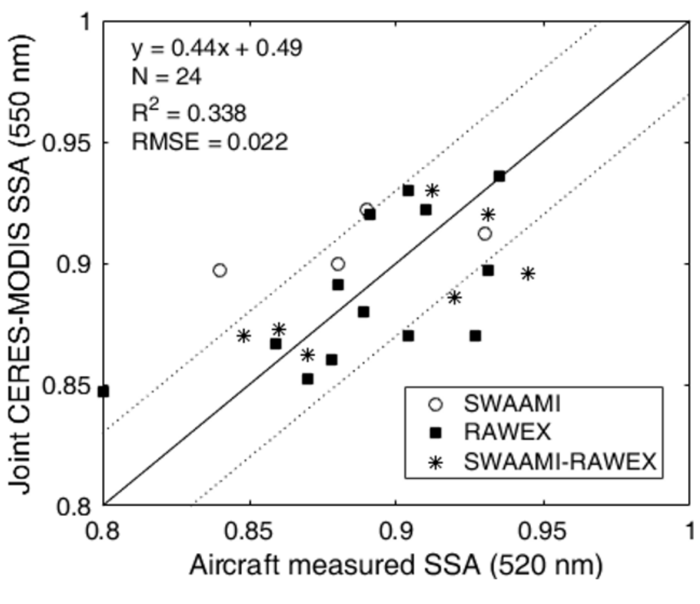

Figure 4. Validation of combined CERES-MODIS SSA with aircraft measurements during SWAAMI, RAWEX, and SWAAMI-RAWEX campaigns. The solid line shows the ideal 1:1 case and dotted lines represent the absolute difference of 0.03.

Most of the points were within the absolute difference of 0.03. However, there are few exceptions. SSA values over the Bay of Bengal during SWAAMI campaign were reported as 0.84 $\pm$ 0.07 during June-July by Manoj et al. (2019), whereas CERES-MODIS retrieves a higher SSA of ~0.89 for the same time period. This large variation could be due to frequent cloud cover during the monsoon season, leading to fewer SSA points retrieved over the ocean and land. SSA estimated over Nagpur in Central India during RAWEX is ~0.8, while CERES-MODIS retrieves ~0.85. This inconsistency is due to the large surface albedo variations (standard deviation >0.05) over Central India, which leads to fewer points available for retrieval. Except for few such cases, most of the other points lie within an absolute difference of 0.03.

For comparison purposes, many previous studies have used ground-level SSA data from AERONET obtained through inversion methods (Zhu et al., 2011; Jethva et al., 2014). Even in this study, only very few points were available for validation due to the limited number of direct measurements of columnar SSA. Despite this limitation, this validation exercise provided confidence to generate global maps of SSA following this method.

5 Results and discussion

Panels a, c, e, and g in Fig. 5 show the seasonal-mean global maps of SSA (550 nm) retrieved by the combined CERES-MODIS algorithm for the five years of 2014-2018. For comparison, Ozone Monitoring Instrument (OMI) SSA at 500 nm (OMAERUVd V3) (Torres et al., 2007; Torres et al., 2013; Ahn et al., 2014), the most widely used global SSA dataset, for the corresponding period are shown in panels b, d, f, and h. Data are averaged for different seasons: DJF (December-January-February), MAM (March-April-May), JJA (June-July-August), and SON (September-October-November).

SSA in the visible region (550 nm) is directly retrieved in the CERES-MODIS algorithm, whereas OMI retrieves SSA primarily in the UV regions and extrapolates them to visible (500 nm) using aerosol models. For a generalized qualitative comparison, we can assume that SSA does not vary much for the small 50 nm spectral difference between CERES-MODIS and OMI SSA. (Zhu et al., 2011; Jethva et al., 2014).

From a quick comparison between the CERES-MODIS and OMI SSA maps, the following points can be noted:

- OMI SSA is susceptible to cloud contamination due to its large footprint size of 13 × 24 km^2, leading to fewer points in the retrieved SSA map. In comparison, we can notice that CERES-MODIS SSA has a

https://doi.org/10.5194/acp-2021-521
Preprint. Discussion started: 27 July 2021

better data coverage on a global scale; absence of data is mostly over regions of persistent cloud coverage or due to the unavailability of MODIS AOD.

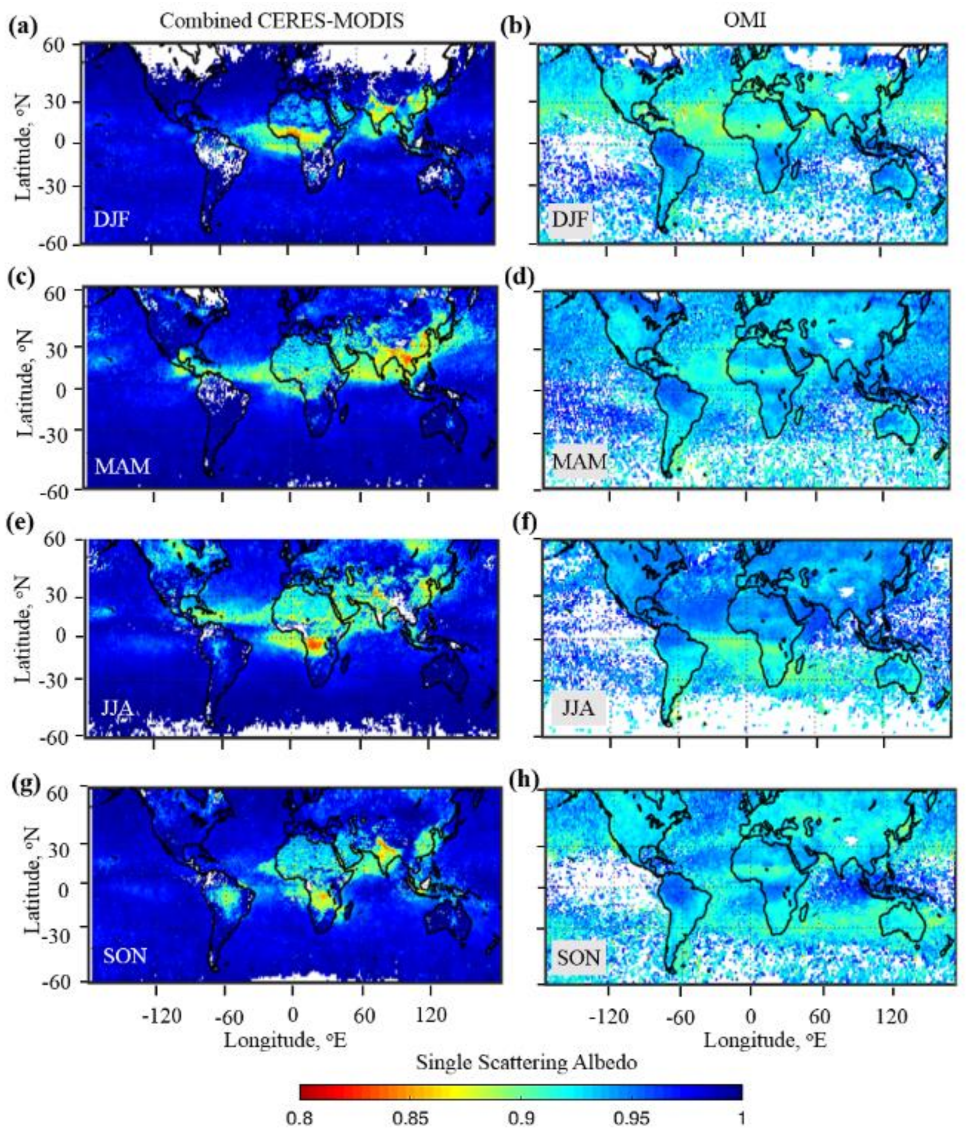

Figure 5. Seasonal mean SSA maps for the period of 2014-18 retrieved by the combined CERES-MODIS algorithm (panels a, c, e and g) and OMI (b, d, f and h).

https://doi.org/10.5194/acp-2021-521
Preprint. Discussion started: 27 July 2021

- The Global Ocean, a relatively dark surface covering more than 70% of the Earth's surface, plays a significant role in determining global aerosol radiative forcing effects. Therefore, the better data coverage over oceans by the CERES-MODIS algorithm provides better input for radiative forcing calculations.

- CERES-MODIS maps capture a wider range of SSA values. Regions with very low SSA can easily be identified as the sources of absorbing aerosols. OMI SSA values are mostly above 0.9 and do not clearly capture the sources and transport of absorbing aerosols.

Global mean SSA retrieved by combined CERES-MODIS over land and ocean is 0.93 and 0.97, respectively (OMI: 0.94 and 0.94). But accurate SSA estimations are also required over regional scales. Hence, seasonal mean SSA values retrieved by the combined CERES-MODIS algorithm are reported here, in table 1, for major regions of interest such as deserts, oceans, biomass-burning forests, and highly polluted industrial areas. Additional details of the regions considered are provided in the supplementary file (Table S1 and Fig. S1). These regions were chosen so as to quantitatively emphasize the ability of CERES-MODIS to better capture the seasonal variations in SSA, where the OMI shows minor variations across seasons.

JJA is marked by a large-scale outbreak of forest fires in the Boreal Forests and South Africa (Justice et al., 1996; Wooster, 2004). While the Canadian boreal forests have mean SSA values of 0.96 in MAM and 0.94 in SON, it reduces to 0.91 during the forest fire season in JJA. Similarly, the Russian boreal forests have higher SSA values (~0.96) during MAM but 0.90 in JJA. The rainforest in Central Africa, being the largest biomass-burning region, shows large variations in SSA from 0.92 in MAM to values as low as 0.8 during JJA. Amazon forest has higher SSA values during MAM (~0.97) and lowest values during its forest fire season in SON (~0.93). These seasonal trends and their associated low SSA values are clearly captured in CERES-MODIS retrieved SSA values. In contrast, OMI fails to show any noticeable trend with values above 0.9 throughout the year.

The North and South Atlantic Oceans are major channels for dust and smoke transport from Africa (Bergstrom et al., 2003). Seasonal trends in SSA retrieved by CERES-MODIS over the Atlantic Ocean are dependent on the biomass burning in Africa, dust-storms in the Sahara, and the wind pattern (Torres et al., 2005). While the SON values are dominated mostly by dust transport from Sahara and have SSA around 0.92, smoke from forest fires over the Atlantic Ocean gives lower SSA (0.89) in JJA. The higher OMI SSA values (~0.95) in the North Atlantic Ocean during JJA could be due to the frequent cloud coverage leading to fewer data points.

https://doi.org/10.5194/acp-2021-521
Preprint. Discussion started: 27 July 2021

Compared to the Atlantic Ocean, the North-eastern Pacific Ocean is a less polluted region, with the CERES-MODIS SSA values mostly above 0.95. However, OMI shows large variations in SSA from 0.99 to 0.92. CERES-MODIS method is most effective when there are large variations in AOD. Hence, higher SSA values may be retrieved over a less polluted oceanic region.

Table 1. Seasonal mean SSA over regions of interest from combined CERES-MODIS and OMI (given in brackets). Details of these regions are given in Table S1 and Fig. S1

Region	CERES-MODIS SSA 550 nm (OMI SSA 500 nm)			
	DJF	MAM	JJA	SON
Canadian Boreal Forest	(0.95 ± 0.02)	0.96 ± 0.02 (0.94 ± 0.01)	0.91 ± 0.02 (0.94 ± 0.01)	0.94 ± 0.02 (0.93 ± 0.01)
Russian Boreal Forest	(0.95 ± 0.02)	0.96 ± 0.02 (0.94 ± 0.01)	0.90 ± 0.01 (0.94 ± 0.01)	0.96 ± 0.01 (0.93 ± 0.01)
South African Forest	0.91 ± 0.02 (0.93 ± 0.01)	0.92 ± 0.01 (0.94 ± 0.01)	0.83 ± 0.01 (0.93 ± 0.02)	0.90 ± 0.01 (0.94 ± 0.01)
Amazon Forest	0.96 ± 0.02 (0.95 ± 0.01)	0.98 ± 0.01 (0.95 ± 0.01)	0.97 ± 0.02 (0.93 ± 0.01)	0.89 ± 0.02 (0.94 ± 0.01)
North East Atlantic	0.96 ± 0.02 (0.90 ± 0.01)	0.94 ± 0.02 (0.92 ± 0.01)	0.92 ± 0.02 (0.95 ± 0.01)	0.93 ± 0.03 (0.94 ± 0.01)
South East Atlantic	0.92 ± 0.02 (0.92 ± 0.01)	0.94 ± 0.02 (0.92 ± 0.01)	0.89 ± 0.01 (0.91 ± 0.01)	0.92 ± 0.02 (0.94 ± 0.01)
Eastern Pacific	0.97 ± 0.01 (0.94 ± 0.02)	0.97 ± 0.01 (0.95 ± 0.02)	0.96 ± 0.01 (0.95 ± 0.02)	0.97 ± 0.01 (0.95 ± 0.02)
Sahara	0.93 ± 0.01 (0.92 ± 0.01)	0.93 ± 0.01 (0.93 ± 0.01)	0.91 ± 0.02 (0.94 ± 0.01)	0.92 ± 0.02 (0.93 ± 0.01)
Indo Gangetic Plain	0.88 ± 0.01 (0.92 ± 0.01)	0.87 ± 0.01 (0.92 ± 0.01)	0.85 ± 0.02 (0.95 ± 0.01)	0.83 ± 0.01 (0.92 ± 0.01)
Eastern China	0.92 ± 0.01 (0.92 ± 0.01)	0.90 ± 0.01 (0.94 ± 0.01)	0.87 ± 0.01 (0.95 ± 0.01)	0.88 ± 0.02 (0.93 ± 0.01)
Arabian Sea	0.92 ± 0.01 (0.91 ± 0.02)	0.89 ± 0.01 (0.93 ± 0.01)	0.91 ± 0.01 (0.96 ± 0.01)	0.89 ± 0.01 (0.93 ± 0.02)
Bay of Bengal	0.91 ± 0.01 (0.92 ± 0.01)	0.90 ± 0.01 (0.94 ± 0.01)	0.91 ± 0.02 (0.95 ± 0.01)	0.91 ± 0.02 (0.94 ± 0.02)

Over the Sahara, there is a reasonable agreement between OMI and CERES-MODIS SSA values. During JJA, smoke over the Sahara can reduce SSA values to 0.89. In other seasons, both CERES-MODIS and OMI give similar SSA values around 0.93. This could indicate that both the algorithms retrieve similar SSA over desert regions. These values are comparable with various other measurements and campaigns over the Sahara (Kaufman et al., 2001; Haywood et al. 2001; Deepshikha et al., 2005).

Eastern China is one of the largest polluted industrial regions. CERES-MODIS SSA shows very low values of 0.87, with the lower values observed mainly during JJA. Whereas OMI shows consistent SSA above 0.9 (with a mean value of ~0.93). Likewise, the Indo-Gangetic plain in India is a densely populated region spotted with several coal-based thermal power plants and seasonal stubble burning. The retrieved SSA values were mostly below 0.89 throughout the year, with values as low as 0.81 during SON. While OMI SSA values are above 0.9.

Thus, the combined CERES-MODIS algorithm better captures the spatial and seasonal trend in aerosol absorption (both sources and transport of aerosols) and provides an improved global SSA database with fewer data gaps.

Overall, the sensitivity of the algorithm depends on the combination of surface albedo, water vapor, and SSA values. Uncertainty is higher for those combinations that give a slope close to zero during the linear regression between CERES $\Delta\alpha$ and MODIS AOD. The average uncertainty is $\pm$0.03, with maximum sensitivity to changes in surface albedo. The uncertainties are higher for scattering aerosols over bright surfaces and absorbing aerosols above dark surfaces. Sensitivity to water vapor is almost negligible, except in very few cases where the uncertainty is $\pm$ 0.008. The CERES-MODIS algorithm is most effective over regions with large AOD variations and less surface albedo variations. A detailed analysis of this method's uncertainties is out of the scope of this paper and will be examined in future studies.

6. Summary and Conclusions

- Global maps of aerosol absorption have been generated following the concept of "critical optical depth".
- The retrieved SSA values have been validated by comparing against available aircraft measurements. The validation exercise shows that most of the retrieved SSA values are within $\pm$0.03.
- We show that the combined CERES-MODIS algorithm better captures the spatial and seasonal variations in aerosol absorption and the resultant maps provide an improved global SSA database with fewer data gaps. Global mean SSA was estimated to be 0.93 and 0.97 over land and ocean, respectively
- The uncertainty analysis shows typical uncertainty of $\pm$0.03, with maximum sensitivity to changes in surface albedo. The algorithm is shown to be the most effective over regions with large AOD variations and less surface albedo variations.

https://doi.org/10.5194/acp-2021-521
Preprint. Discussion started: 27 July 2021

- Overall, the combined CERES-MODIS algorithm provides global SSA maps with improved accuracy and better spatial coverage. These global maps provide valuable input for models to make assessment of aerosol-climate impacts on both regional and global scales.

Data Availability

MODIS and CERES data used in this study are available at https://asdc.larc.nasa.gov/

Author Contributions

SKS conceptualized the method. AD developed the algorithm, carried out the simulations, and analyzed the data. AD wrote the manuscript with revisions from SKS.

Competing interests

The authors declare they have no conflict of interest.

Acknowledgment

The authors gratefully acknowledge the Atmospheric Science Data Center (ASDC) at NASA's Earth Observing System Data and Information System (EOSDIS) Distributed Active Archive Centers (DAACs) for providing MODIS, OMI, and CERES data products used in this study. In addition, one of the authors (S. K. Satheesh) acknowledges the JC Bose Fellowship awarded to him by SERB-Department of Science and Technology, New Delhi. This study is supported by "Tata Education and Development Trust."

References

Ahn, C., Torres, O. and Jethva, H.: Assessment of OMI near-UV aerosol optical depth over land, J. Geophys. Res. Atmos., 119(5), 2457–2473, https://doi.org/10.1002/2013JD020188, 2014.

Anderson, T. L., Charlson, R. J., Bellouin, N., Boucher, O., Chin, M., Christopher, S. A., Haywood, J., Kaufman, Y. J., Kinne, S., Ogren, J. A., Remer, L. A., Takemura, T., Tanré, D., Torres, O., Trepte, C. R., Wielicki, B. A., Winker, D. M. and Yu, H.: An "a-train"strategy for quantifying direct climate forcing by anthropogenic aerosols, Bull. Am. Meteorol. Soc., 86(12), 1795–1809, doi:10.1175/BAMS-86-12-1795, 2005.

Babu, S. S., Moorthy, K. K., Manchanda, R. K., Sinha, P. R., Satheesh, S. K., Vajja, D. P., Srinivasan, S. and Kumar, V. H. A.: Free tropospheric black carbon aerosol measurements using high altitude balloon: Do BC layers build "their own homes"up in the atmosphere?, Geophys. Res. Lett., 38(8), doi:10.1029/2011GL046654, 2011.

Babu, S. S., Nair, V. S., Gogoi, M. M. and Moorthy, K. K.: Seasonal variation of vertical distribution of aerosol single scattering albedo over Indian sub-continent: RAWEX aircraft observations, Atmos. Environ., 125, 312–323, doi:10.1016/j.atmosenv.2015.09.041, 2016.

Bergstrom, R. W., Pilewskie, P., Schmid, B. and Russell, P. B.: Estimates of the spectral aerosol single scattering albedo and aerosol radiative effects during SAFARI 2000, J. Geophys. Res. Atmos., 108(D13), https://doi.org/10.1029/2002JD002435, 2003.

IPCC – Intergovernmental Panel on Climate Change: The physical science basis: Contribution of Working Group I to the Fifth Assessment Report of the Intergovernmental Panel on Climate Change, in: Climate Change (2013), edited by: Stocker, T. F., Qin, D., Plattner, G. K., Tignor, M., Allen, S. K., Boschung, J., Nauels, A., Xia, Y., Bex, V., and Midgley, P. M., Cambridge University, Press, Cambridge, UK and New York, NY, USA, 1535 pp., https://doi.org/10.1017/CBO9781107415324, 2013.

Chand, D., Wood, R., Anderson, T. L., Satheesh, S. K., and Charlson, R. J.: Satellite-derived direct radiative effect of aerosols dependent on cloud cover, Nat. Geosci., 2, 181–184, https://doi.org/10.1038/ngeo437, 2009.

Deepshikha, S., Satheesh, S. K. and Srinivasan, J.: Regional distribution of absorbing efficiency of dust aerosols over India and adjacent continents inferred using satellite remote sensing, Geophys. Res. Lett., 32(3), 1–4, doi:10.1029/2004GL022091, 2005.

Dubovik, O., Holben, B., Eck, T. F., Smirnov, A., Kaufman, Y. J., King, M. D., Tanré, D., and Slutsker, I.: Variability of Absorption and Optical Properties of Key Aerosol Types Observed in Worldwide Locations. Journal of the Atmospheric Sciences 59, 3, 590-608, https://doi.org/10.1175/1520-0469(2002)059<0590:VOAAOP>2.0.CO;2, 2002

Eswaran, K., Satheesh, S. K. and Srinivasan, J.: Multi-satellite retrieval of single scattering albedo using the OMI–MODIS algorithm, Atmos. Chem. Phys., 19(5), 3307–3324, doi:10.5194/acp-19-3307-2019, 2019.

Fraser, R. S. and Kaufman, Y. J, "The Relative Importance of Aerosol Scattering and Absorption in Remote Sensing," in IEEE Transactions on Geoscience and Remote Sensing, vol. GE-23, no. 5, pp. 625-633, Sept. 1985, doi: 10.1109/TGRS.1985.289380.

Govardhan, G., Satheesh, S. K., Moorthy, K. K. and Nanjundiah, R.: Simulations of black carbon over the Indian region: improvements and implications of diurnality in emissions, Atmos. Chem. Phys., 19(12), 8229–8241, doi:10.5194/acp-19-8229-2019, 2019.

Haywood, J. M., Francis, P. N., Glew, M. D. and Taylor, J. P.: Optical properties and direct radiative effect of Saharan dust: A case study of two Saharan dust outbreaks using aircraft data, J. Geophys. Res. Atmos., 106(D16), 18417–18430, doi:10.1029/ 2000JD900319 @10.1002/ (ISSN)2169-8996.DUST1, 2001.

Hammer, M. S., Martin, R. V., Li, C., Torres, O., Manning, M., and Boys, B. L.: Insight into global trends in aerosol composition from 2005 to 2015 inferred from the OMI Ultraviolet Aerosol Index, Atmos. Chem. Phys., 18, 8097–8112, https://doi.org/10.5194/acp-18-8097-2018, 2018.

Hsu, N. C., Herman, J. R. and Weaver, C.: Determination of radiative forcing of Saharan dust using combined TOMS and ERBE data, J. Geophys. Res. Atmos., 105(16), 20649–20661, doi:10.1029/2000jd900150, 2000.

Hsu, N. C., Tsay, S. C., King, M. D. and Herman, J. R.: Aerosol properties over bright-reflecting source regions, IEEE Trans. Geosci. Remote Sens., 42(3), 557–569, doi:10.1109/TGRS.2004.824067, 2004.

Jethva, H., Torres, O., and Ahn, C.: A 12-year long global record of optical depth of absorbing aerosols above the clouds derived from the OMI/OMACA algorithm, Atmos. Meas. Tech., 11, 5837–5864, https://doi.org/10.5194/amt-11-5837-2018, 2018.

Jethva, H. and Torres, O.: A comparative evaluation of Aura-OMI and SKYNET near-UV single-scattering albedo products, Atmos. Meas. Tech., 12(12), 6489–6503, https://doi.org/10.5194/amt-12-6489-2019, 2019.

Justice, C. O., Kendall, J. D., Dowty, P. R. and Scholes, R. J.: Satellite remote sensing of fires during the SAFARI campaign using NOAA Advanced Very High Resolution Radiometer data, J. Geophys. Res. Atmos., 101(D19), 23851–23863, https://doi.org/10.1029/95JD00623, 1996.

Hsu, N. C., Jeong, M. J., Bettenhausen, C., Sayer, A. M., Hansell, R., Seftor, C. S., Huang, J., and Tsay, S. C.: Enhanced Deep Blue aerosol retrieval algorithm: The second generation, J. Geophys. Res. Atmos., 118, 9296–9315, https://doi.org/10.1002/jgrd.50712, 2013.

Hu, R. -M., Martin, R. V. and Fairlie, T. D.: Global retrieval of columnar aerosol single scattering albedo from space-based observations, J. Geophys. Res. Atmos., 112(D2), doi:10.1029/2005JD006832, 2007.

Hu, R. M., Sokhi, R. S. and Fisher, B. E. A.: New algorithms and their application for satellite remote sensing of surface PM2.5 and aerosol absorption, J. Aerosol Sci., 40(5), 394–402, doi:10.1016/j.jaerosci.2009.01.005, 2009.

Jeong, M. J. and Hsu, N. C.: Retrievals of aerosol single-scattering albedo and effective aerosol layer height for biomass-burning smoke: Synergy derived from "A-Train"sensors, Geophys. Res. Lett., 35(24), L24801, doi:10.1029/2008GL036279, 2008.

Kaufman, Y. J.: Satellite sensing of aerosol absorption., J. Geophys. Res., 92(D4), 4307–4317, doi:10.1029/JD092iD04p04307, 1987.

Kaufman, Y. J. and Joseph, J. H.: Determination of surface albedos and aerosol extinction characteristics from satellite imagery., J. Geophys. Res., 87(C2), 1287–1299, https://doi.org/10.1029/JC087iC02p01287, 1982.

Kaufman, Y. J., Tanré, D. and Boucher, O.: A satellite view of aerosols in the climate system, Nature, 419(6903), 215–223, https://doi.org/10.1038/nature01091, 2002.

Kaufman, Y. J., Tanré, D., Dubovik, O., Karnieli, A. and Remer, L. A.: Absorption of sunlight by dust as inferred from satellite and ground-based remote sensing, Geophys. Res. Lett., 28(8), 1479–1482, doi:10.1029/2000GL012647, 2001.

Lenoble, J., Remer, L. and Tanre, D. eds.: Aerosol remote sensing. Springer Science & Business Media, 2013.

Levy, R. C., Remer, L. A., Mattoo, S., Vermote, E. F. and Kaufman, Y. J.: Second-generation operational algorithm: Retrieval of aerosol properties over land from inversion of Moderate Resolution Imaging Spectroradiometer spectral reflectance, J. Geophys. Res. Atmos., 112(13), doi:10.1029/2006JD007811, 2007.

Levy, R. C., Remer, L. A., and Dubovik, O.: Global aerosol optical properties and application to Moderate Resolution Imaging Spectroradiometer aerosol retrieval over land, J. Geophys. Res. Atmos., 112, 13210, https://doi.org/10.1029/2006JD007815, 2007.Levy, R. C., Mattoo, S., Munchak, L. A., Remer, L. A., Sayer, A. M., Patadia, F. and Hsu, N. C.: The Collection 6 MODIS aerosol products over land and ocean, Atmos. Meas. Tech., 6(11), 2989–3034, doi:10.5194/amt-6-2989-2013, 2013.

Manoj, M. R., Satheesh, S. K., Moorthy, K. K. and Coe, H.: Vertical profiles of sub-micron aerosol single scattering albedo over Indian region immediately before monsoon onset and during its development: Research from the SWAAMI field campaign, Atmos. Chem. Phys. Discuss., 1–29, doi:10.5194/acp-2019-657, 2019.

Moorthy, K. K., Satheesh, S. K. and Kotamarthi, V. R.: Evolution of aerosol research in India and the RAWEX–GVAX: an overview, Curr. Sci., 111, 53–75, doi:10.2307/24910009, n.d.

Narasimhan, D. and Satheesh, S. K.: Estimates of aerosol absorption over India using multi-satellite retrieval, Ann. Geophys., 31(10), 1773–1778, doi:10.5194/angeo-31-1773-2013, 2013.

Rutan, D. A., Kato, S., Doelling, D. R., Rose, F. G., Nguyen, L. T., Caldwell, T. E. and Loeb, N. G.: CERES Synoptic Product: Methodology and Validation of Surface Radiant Flux, J. Atmos. Ocean. Technol., 32(6), 1121–1143, doi:10.1175/JTECH-D-14-00165.1, 2015.

Remer, L. A., Kleidman, R. G., Levy, R. C., Kaufman, Y. J., Tanré, D., Mattoo, S., Martins, J. V., Ichoku, C., Koren, I., Yu, H., and Holben, B. N.: Global aerosol climatology from the MODIS satellite sensors, J. Geophys. Res. Atmos., 113, 14–21, https://doi.org/10.1029/2007JD009661, 2008.

Satheesh, S. K. and Srinivasan, J.: A method to infer short wave absorption due to aerosols using satellite remote sensing, Geophys. Res. Lett., 32(13), 1–4, doi:10.1029/2005GL023064, 2005.

Satheesh, S. K., Krishna Moorthy, K., Suresh Babu, S., Vinoj, V. and Dutt, C. B. S.: Climate implications of large warming by elevated aerosol over India, Geophys. Res. Lett., 35(19), L19809, doi:10.1029/2008GL034944, 2008.

Satheesh, S. K., Torres, O., Remer, L. A., Babu, S. S., Vinoj, V., Eck, T. F., Kleidman, R. G. and Holben, B. N.: Improved assessment of aerosol absorption using OMI-MODIS joint retrieval, J. Geophys. Res. Atmos., 114(5), D05209, doi:10.1029/2008JD011024, 2009.

Sayer, A. M., Hsu, N. C., Bettenhausen, C. and Jeong, M. J.: Validation and uncertainty estimates for MODIS Collection 6 “deep Blue”aerosol data, J. Geophys. Res. Atmos., 118(14), 7864–7872, doi:10.1002/jgrd.50600, 2013.

Stamnes, K., Tsay, S.-C., Wiscombe, W. and Jayaweera, K.: Numerically stable algorithm for discrete-ordinate-method radiative transfer in multiple scattering and emitting layered media, Appl. Opt., 27(12), 2502, doi:10.1364/ao.27.002502, 1988.

Torres, O., Bhartia, P. K., Herman, J. R., Sinyuk, A., Ginoux, P. and Holben, B.: A long-term record of aerosol optical depth from TOMS observations and comparison to AERONET measurements, J. Atmos. Sci., 59(3 PT 1), 398–413, https://doi.org/10.1175/1520-0469(2002)059<0398:altroa>2.0.co;2, 2002.

Torres, O., Bhartia, P.K., Sinyuk, A., Welton, E.J. and Holben, B.: Total Ozone Mapping Spectrometer measurements of aerosol absorption from space: Comparison to SAFARI 2000 ground-based observations. Journal of Geophysical Research: Atmospheres, 110(D10), 2005.

Torres, O., Tanskanen, A., Veihelmann, B., Ahn, C., Braak, R., Bhartia, P. K., Veefkind, P., and Levelt, P.: Aerosols and surface UV products from Ozone Monitoring Instrument observations: An overview, J. Geophys. Res. Atmos., 112, https://doi.org/10.1029/2007JD008809@10.1002/(ISSN)2169-8996.AURA1, 2007.

Torres, O., Ahn, C. and Chen, Z.: Improvements to the OMI near-UV aerosol algorithm using A-train CALIOP and AIRS observations, Atmos. Meas. Tech., 6(11), 3257–3270, https://doi.org/10.5194/amt-6-3257-2013, 2013.

Vaishya, A., Babu, S. N. S., Jayachandran, V., Gogoi, M. M., Lakshmi, N. B., Moorthy, K. K. and Satheesh, S. K.: Large contrast in the vertical distribution of aerosol optical properties and radiative effects across the Indo-Gangetic Plain during the SWAAMI–RAWEX campaign, Atmos. Chem. Phys., 18(23), 17669–17685, doi:10.5194/acp-18-17669-2018, 2018.

Wielicki, B. A., Barkstrom, B. R., Harrison, E. F., Lee, R. B., Smith, G. L. and Cooper, J. E.: Clouds and the Earth's Radiant Energy System (CERES): An Earth Observing System Experiment, Bull. Am. Meteorol. Soc., 77(5), 853–868, doi:10.1175/1520-0477(1996)077<0853:CATERE>2.0.CO;2, 1996.

Wooster, M. J.: Boreal forest fires burn less intensely in Russia than in North America, Geophys. Res. Lett., 31(20), L20505, https://doi.org/10.1029/2004GL020805, 2004.

Zhu, L., Martins, J. V. and Remer, L. A.: Biomass burning aerosol absorption measurements with MODIS using the critical reflectance method, J. Geophys. Res. Atmos., 116(7), D07202, doi:10.1029/2010JD015187, 2011.